Phase transitions and anisotropic responses of planar triangular nets under large deformation

Dennis E. Discher,* David H. Boal, and S. K. Boey
Department of Physics, Simon Fraser University, Burnaby, British Columbia, Canada V5A 1S6
(Received 18 September 1996)

Responses of triangular networks in large reversible deformation are studied analytically at zero temperature and by Monte Carlo simulation at nonzero temperature. Exact expressions for the elastic strain energy at zero temperature are derived for several models in which the network potential energy depends on either the length of the network element (i.e., central force interactions) and/or the area of each network triangle. For nets of Hookean spring elements having a nonzero force-free length, cubic terms arise in the strain energy through the sixfold symmetry of the network, and thereby break the symmetric response at small strain. Because of the symmetry of the two-body potential and the anisotropy of the network, pure compression of the Hookean spring net leads to a martensiticlike phase transition at all finite temperatures studied. Networks of elemental tethers or springs that have a zero force-free length balanced against a three-vertex potential energy that rises with decreasing triangle area (to emulate volume exclusion in polymer networks) do not undergo a phase transition, although inclusion of a maximum tether length (to model the polymer chains' contour limits) reveals a simple but distinct type of triangular net anisotropy. [S1063-651X(97)10104-0]

PACS number(s): 03.20.+i, 87.22.Bt, 68.60.Bs, 64.70.−p

I. INTRODUCTION

A remarkable feature of planar structures with local sixfold symmetry is that they *can* appear mechanically isotropic regardless of other intrinsic properties (see, for example, Ref. [1]). Elastic sixfold structures thus can be assembled from identical elements having arbitrary interactions, and yet such structures require just two isotropic material constants (e.g., shear modulus and compressibility) to describe their response adequately within at least some small regime of strain. This fact is especially pertinent to understanding a range of sixfold structures including ultrasoft cell membrane cytoskeletons [2–4] and certain thin, nanostructured C_6-symmetric sheets [5]. Such structures raise the natural question: under what conditions and in what ways does the mechanical response begin to reflect more of the underlying sixfold symmetry?

The present work focuses on triangulated network models under large, elastic deformation. As a partial motivation for this study, mesoscopic views of real cell membrane cytoskeletons in deformation show them to be capable of sustaining very large strains, including very large compressive strains [3]. In the conventional thinking about elasticity as an energy expansion in a strain measure, large deformation introduces higher-order terms which are associated with a range of phenomena. One of the most remarkable and long studied is the martensitic transition which refers to a structural, reordering transformation in which no atomic diffusion is thought to occur [6]. Many such transitions, useful for smart materials [6], are held to be strongly first order because of cubic strain terms in the free energy [7]. However, in some of the driven martensitic transitions, particularly those in which moderately large displacements (~10% strains) occur, diffusion may not be completely absent [8]. Unlike noncovalently bonded systems, the networked systems analyzed here are permanently tethered together, and strictly maintain their connectivity and topology, by explicit construction, even at infinite temperatures. Thus all geometric transformations of the network occur in the absence of long-range diffusion.

Triangulated networks are assembled from linear elements or bonds joined at sixfold junctions [Fig. 1(a)]. The linear elements are infinitely thin hard rods in the sense that they are not permitted to overlap except at the sixfold vertices [9]. At this microscopic level, energetics could be a function of (i) the distance between vertices (i.e., central force interactions), (ii) the area of a triangle circumscribed by elements, and/or (iii) the angle between elements such as in a Keating potential [10]. In this work we consider only the simplest, nearest-neighbor examples of the first two types of interactions, the latter of which has been examined only in other contexts [11]. Also, whereas similar networks fluctuating in three dimensions have been studied in efforts at understanding aspects of thermal bending undulations and plane-projection elasticity [12] in addition to so-called stretching ridges arising in bending [13], only in-plane motions of the network junction points or particles are permitted in the present studies. At least one unusual material feature, a negative Poisson ratio, is already known to arise when a moderate isotropic tension is applied to such planar triangular nets of (i) Hookean springs having nonzero resting lengths or (ii) network elements having only a finite maximum length (i.e., square-well potentials) [9].

Before outlining the format of the present paper, we first very briefly introduce what may be the most interesting finding in this work. A simple, planar triangular network of springs of fluctuating length S is once more considered. The elemental energetics are, in this case, assigned the innocuous-looking Hookean form $U=\frac{1}{2}k_{sp}(S-S_0)^2$, where k_{sp} is the fixed spring constant and S_0 is the fixed rest length. Under a compressive network pressure P, a discontinuity appears in the average network area, $\langle A\rangle$ [Fig. 1(b)] over a

*Present address: University of Pennsylvania, 297 Towne Bldg., Philadelphia, PA 19104-6315.

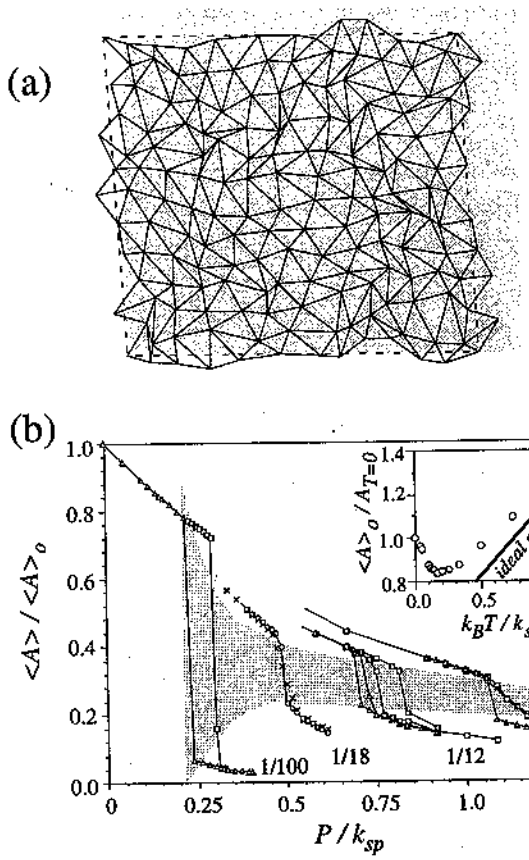

FIG. 1. Finite-temperature simulations of Hookean spring networks under zero stress or compression. (a) Sample configuration of an unstressed Hookean spring net ($N=12^2$; $P=0$; $k_BT/k_{sp}S_0^2=\frac{1}{12}$) in a periodic box (dashed line). The underlying gray rectangle with sides ($S_0\sqrt{N}$) by $[(\sqrt{3}/2)S_0\sqrt{N}]$ defines the zero-temperature area $A_{T=0}=N(\sqrt{3}/2)S_0^2$. (b) Low-temperature isotherms on the compression half of the plane. Temperatures given under each set of curves are in dimensionless units of $k_BT/k_{sp}S_0^2$. Squares indicate simulations that were started in the above rectangular state. Triangles indicate simulations that were started in a state where the long side of the box was 1.33 ($S_0\sqrt{N}$), and the short side was 0.05 $[(\sqrt{3}/2)S_0\sqrt{N}]$. The system size for the lowest temperature of $\frac{1}{100}$ was $N=4^2$. The system sizes for the temperature of $\frac{1}{18}$ were $N=6^2$ (crosses) and $N=8^2$ (circles); hysteresis was minimal for these two system sizes. The system sizes for the temperature of $\frac{1}{12}$ were $N=8^2$ (inner loop) and $N=16^2$ (outer loop). The system size for the temperature of $\frac{1}{9}$ was $N=24^2$; a system of size $N=12^2$ showed undetectable hysteresis. The inset figure gives, as a function of temperature, the stress-free area $\langle A\rangle_0$ scaled by $A_{T=0}$. Corresponding to ideal gas behavior as described in the text, the slope of the heavy line is $\frac{2}{3}$. Lines through the simulation data are drawn to guide the eye.

wide range of fixed temperatures $T=k_{sp}S_0^2/k_B$ (where k_B is Boltzmann's constant). These results are obtained by Monte Carlo simulations in which each of N nodal particles of the net is moved within the plane according to the usual Boltzmann weighting scheme [9]. The geometry (area and shape) of the periodic box, as conjugate to a set pressure, is allowed to fluctuate through collective, affine motions of the nodes. Detailed features of the noted phase transition, such as hysteresis, are elaborated upon in the remainder of this paper along with an effort to rationalize the phenomena within the

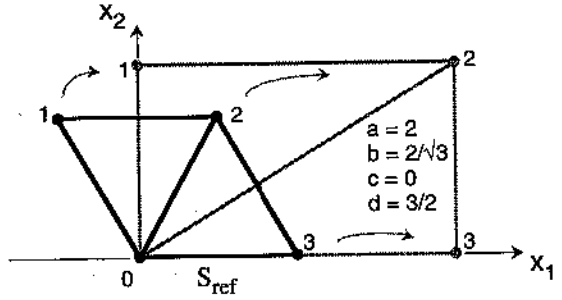

FIG. 2. Sample deformation of a plaquette parallelogram from the reference configuration where all elemental lengths are S_{ref}.

context of more general models and mean-field ideas including large deformation elasticity and Landau theory. Particular attention is given to anisotropic responses which arise from the sixfold symmetry of various network models including one class of Hamiltonians which is introduced as an effective representation of a triangular network of self-avoiding polymer chains.

The format of the paper is as follows: first, formalisms and definitions of large deformation elasticity as applied to triangular networks, including geometric and energetic ideas, are enumerated in Sec. II. Then, as the first of three specific models within a general class of Hamiltonians, the Hookean spring net is thoroughly studied in Sec. III at selected temperatures from zero to infinity and, most notably, under compression. In Sec. IV, square-well networks which lack an intrinsic energy scale are studied by both simulation and mean-field methods. Section V introduces and discusses a model closely related to both previous models, but intended to capture distinguishing features of cell membrane cytoskeletons. Conclusions are summarized in Sec. VI.

II. PRELIMINARIES: ELASTICITY OF TRIANGULAR NETS

Large deformation elasticity [14–16] subsumes the more specialized and well-studied theory of infinitesimal deformation (see, for example, Ref. [1]), and proves useful here Application, in Sec. II A, of some of large deformation elasticity's simplest tenets to the homogeneous deformation o triangular networks serves to identify key concepts. Afte first introducing expressions pertinent to network geometry general aspects of the C_6-network response, including zero temperature energetics, are elaborated upon in Sec. II B for particular class of network Hamiltonians. Two calculationa methods are used in our study of networks under large deformation: mean-field approaches are given in Sec. II C while computer simulation techniques for periodicall bounded networks at non-zero temperature and stress ar outlined in Sec. II D.

A. Network deformation

A reference configuration for the deformation is taken t be a unit plaquette with linear material elements all of lengt $|\mathbf{r}_{ij}|=S_{ref}$ (Fig. 2). In deformation, the plaquette is mappe affinely into a new configuration constrained only by $\mathbf{z}\cdot(\mathbf{r}\times\mathbf{r}_{ik})>0$ ($i\neq j\neq k$; no sum on indices of vectors), where is the normal to the plane and definitions of the neares

neighbor vectors should be apparent from the figure. The in-plane deformation map Γ takes the form $x_a=\Gamma_{aB}X_B$ ($a,B=1,2$; sum on repeated indices of tensor components) and, by the definition of affineness, the four components of the tensor Γ are taken to be spatially uniform. The notational convention employed for deformation and stress variables [14–16] is that lower-case letters, including indices, refer to the space of deformed configurations, while capital letters refer to the undeformed or reference configurational space; as the same set of basis vectors is used throughout this work, this convention here serves primarily to emphasize what configurational space, deformed and/or undeformed, a stress or strain quantity belongs to. For simplicity, we designate $a=\Gamma_{11}$, $b=\Gamma_{12}$, $c=\Gamma_{21}$, and $d=\Gamma_{22}$. The distances $|\mathbf{r}_{ij}|=(\mathbf{r}_{ij}\cdot\mathbf{r}_{ij})^{1/2}$ ($i\neq j$) between the particles of Fig. 2 become

$$|\mathbf{r}_{01}|=\tfrac{1}{2}S_{\rm ref}[(-a+b\sqrt{3})^2+(-c+d\sqrt{3})^2]^{1/2},$$

$$|\mathbf{r}_{02}|=\tfrac{1}{2}S_{\rm ref}[(a+b\sqrt{3})^2+(c+d\sqrt{3})^2]^{1/2}, \qquad (1)$$

$$|\mathbf{r}_{03}|=S_{\rm ref}[a^2+c^2]^{1/2}.$$

Setting $c=0$ merely removes a pure rigid body rotation. The density of particles relative to the reference configuration, with one particle per plaquette, may be shown to be $\bar{\rho}=1/\det\Gamma$. A stretch tensor Λ also may be defined through $\Lambda^2=\Gamma^T\Gamma$, so that the roots of the eigenvalues of Λ^2 gives surface stretches λ_I in principal directions. The conventional Lagrangian strain tensor $\mathbf{E}=\frac{1}{2}(\Lambda^2-\mathbf{I})$ [1,14], contains a quadratic term missing in the infinitesimal elasticity theory but essential to keep in large deformation. Components of $\mathbf{E}$ are $E_{11}=\frac{1}{2}(a^2+c^2-1)$, $E_{22}=\frac{1}{2}(b^2+d^2-1)$, and $E_{12}=E_{21}=ab+cd$. In a biaxial deformation, off-diagonal strain components vanish, so that selecting the x and y axes as the principal directions leads to $b=c=0$, $\lambda_1=a$, and $\lambda_2=d$. The stretches may then be approximated by the principal strains E_1 and E_2 as $\lambda_I=1+E_I-\frac{1}{2}E_I^2+\frac{1}{2}E_I^3+\cdots$.

The reference configuration of Fig. 2 can tile a plane and thereby give C_6 symmetry. An irreducible representation for this symmetry group [17] may then be formed from three combinations of the strain components:

$$\eta_1=\text{tr }\mathbf{E},$$

$$\eta_2=\frac{1}{\sqrt{2}}(E_{11}-E_{22}), \qquad (2)$$

$$\eta_3=E_{12}.$$

Each η_i may later be considered a possible order parameter in a Landau theory [17]. Altogether, the η_i form a basis for exactly four independent combinations of deformation measures invariant to transformation of the planar reference state [18],

$$I_1=\text{tr }\mathbf{E}=\eta_1,$$

$$I_2=\det\mathbf{E}=\tfrac{1}{4}\eta_1^2-\tfrac{1}{2}\eta_2^2-\eta_3^2, \qquad (3)$$

$$I_3=E_{11}[(E_{11}+3E_{22})^2-12E_{12}^2]=2\eta_1^3-3\eta_1\eta_2^2+\sqrt{2}\eta_2^3-6\eta_3^2(\eta_1+\eta_2\sqrt{2}),$$

$$I_4=E_{12}[3(E_{11}-E_{22})^2-4E_{12}^2]=2\eta_3(3\eta_2^2-2\eta_3).$$

The latter two invariants are clearly of order $\mathbf{E}^3$, and are particular to the C_6 symmetry. Also, the linear combination $(2I_1+4I_2+1)$ is necessarily an invariant simply equal to $1/\bar{\rho}^2$ and may thus be used in place of either I_1 or I_2.

B. Network response: Hamiltonian and zero-temperature elasticity

Typically, the elastic free energy per reference volume or area is assumed at the outset to be a Taylor expansion in a suitable deformation measure such as the Lagrangian strain (see, for example, Ref. [1])

$$\tilde{W}=\tilde{W}(T,\mathbf{E})=C_{AB}E_{AB}+\frac{1}{2!}C_{ABCD}E_{AB}E_{CD}+\frac{1}{3!}C_{ABCDEF}E_{AB}E_{CD}E_{EF}+\cdots. \qquad (4)$$

As in a Landau theory, a reduction in terms is often achieved by using symmetries of the undeformed structure to simplify the strain energy to a polynomial in invariants, an approach quite general even for large deformation [18]. An isotropic elastic surface is an important example that has an energy written exclusively in terms of I_1 and I_2.

For the present analysis, simple interaction potentials admit a more microscopic starting point than Eq. (4). Networks are assembled from n-monic springs (n even, $n=2$ is harmonic), each having a spring constant $k_{\rm sp}$ (≥ 0) and a resting length S_0 (≥ 0). Also, each triangle of adjacent springs effectively may have a potential energy dependent on the triangulated area. Superposition of these two energy storage modes leads to a general class of discrete system Hamiltonians

$$H=\frac{1}{2!}\sum_{ij}^{\rm net}\frac{1}{n}k_{\rm sp}[(\mathbf{r}_{ij}\cdot\mathbf{r}_{ij})^{1/2}-S_0]^n+\frac{1}{3!}\sum_{ijk}^{\rm net}f(A_{\rm ref}/A_{ijk}). \qquad (5)$$

In this expression, the deformed triangle area is given by the three-vertex quantity $A_{ijk}=\frac{1}{2}|\mathbf{r}_{ij}\times\mathbf{r}_{ik}|$, and the reference triangle area is $A_{\rm ref}=(\sqrt{3}/4)S_{\rm ref}^2$. Thus $\bar{\rho}=A_{\rm ref}/A_{ijk}$ is a spatially independent constant in a homogeneously deformed network. Figure 3 shows some of the potential forms represented by Eq. (5).

In the zero-temperature limit, the average state and other properties are just those, in this case, of perfectly ordered, homogeneous networks. That is, any given plaquette configuration is assumed to be representative of a homogeneously deformed net. Within this limit where ensemble averaging is trivial, and in terms of the elemental lengths and the relative density, an *exact* expression for the elastic strain energy per reference area is

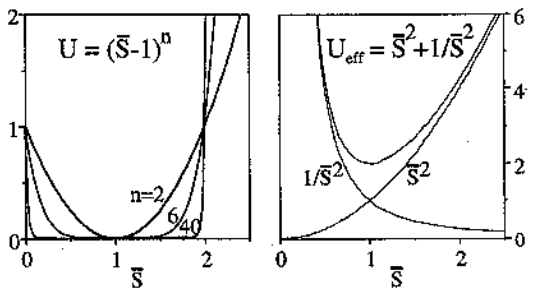

FIG. 3. Dimensionless tether potentials vs dimensionless bond length. Leftmost panel: examples of n-monic tether potentials in which $\bar{S}=S/S_0$, $(1/n)k_{sp}S_0^2/k_BT=1$, and $f(A_{ref}/A_{ijk})=0$. Rightmost panel: effective tether potential when $S_0=0$, $\bar{S}=S/S_{ref}$, $n=2$, $\frac{1}{2}k_{sp}S_{ref}^2/k_BT=1$, and $f(A_{ref}/A_{ijk})$ is taken to be $1/\bar{S}^2$ by assuming equilateral triangles.

$$\tilde{W}=H/2A_{ref}=\left(\frac{\sqrt{3}}{2}S_{ref}^2\right)^{-1}\left\{\frac{1}{n}k_{sp}\sum_{i=1}^{3}(|\mathbf{r}_{0i}|-S_0)^n+f(\bar{\rho})\right\}. \tag{6}$$

The relevant energy scale is $k_{sp}S_{ref}^2/k_BT$, a ratio which goes to infinity in the $T=0$ limit. In this limit, specification of the various microscopic parameters n, k_{sp}, etc. allows one to determine the exact form of the strain energy in terms of desired strain variables, notably invariants of Eq. (3). The tensions (force per length) arising within a network in a given state of strain are then readily calculated from $T_{ab}=\bar{\rho}\,\Gamma_{aC}\partial\tilde{W}/\partial\Gamma_{bC}$, and a two-dimensional internal pressure is identified as $P=-\frac{1}{2}\mathrm{tr}T$. With $\tilde{A}$ as the area of either a plaquette or full network, the compression modulus is then $K_a=-\tilde{A}dP/d\tilde{A}$. Appendix A elaborates some useful simplifications in biaxial deformation.

C. Nonzero pressures and temperatures in mean field

In terms of an applied surface pressure P at zero temperature, the Gibb's free energy per reference area, $\tilde{G}=\tilde{G}(T,P)$, should generally be minimized at equilibrium, in the absence of other constraints. It is simply the Legendre transform of a strain energy density

$$\tilde{G}_{T=0}=\tilde{W}+P/\bar{\rho}. \tag{7}$$

Note that the last term is just the appropriate pressure-area work [for an analysis of martensitic transitions using Eq. (7), see Ref. [19]]. As a function of the biaxial deformation variables a and d, Fig. 4(a) shows the $(1/\bar{\rho})$ surface, which, in Eq. (7), is just the P-scaled second term added to $\tilde{W}$.

For temperatures greater than zero, configurational fluctuations of the representative plaquette (Fig. 2) may be evaluated more rigorously via a partition function Z_P. The model is still a homogeneous net mean-field, model and amounts to an integral over the configuration space (or at least the important regions) mapped out by the plaquette's fluctuating sides. In terms of the coordinates of particles 2 and 3:

$$Z_P=\int x_3dx_3\int dy_2dx_2\exp[(-H+Px_3y_2)/k_BT]. \tag{8}$$

Of note, the expression for Z_P published previously [9] had an incorrect weight for x_3. Z_P is readily reduced to the one-dimensional integral for a fluctuating equilateral triangle by integrating over δ functions at $y_2=(\sqrt{3}/2)x_3$ and $x_2=\frac{1}{2}x_3$. In special cases (see Sec. IV A), the fluctuating equilateral triangle model can be evaluated analytically; numerical integration is otherwise straightforward. The free energy $\tilde{G}=-k_BT\ln Z_P$, as well as thermal averages including the average area per plaquette, $\langle A\rangle=\langle x_3y_2\rangle$, may readily be determined.

Importantly, in the above mean-field models, every plaquette of a network is forced to be the same, hence all interplaquette correlations and stress gradients are explicitly neglected. This restriction is absent in network simulations.

D. Nonzero pressures and temperatures by Monte Carlo simulation

As described briefly in Sec. I, full network simulations can be conducted by Monte Carlo methods over a large tem-

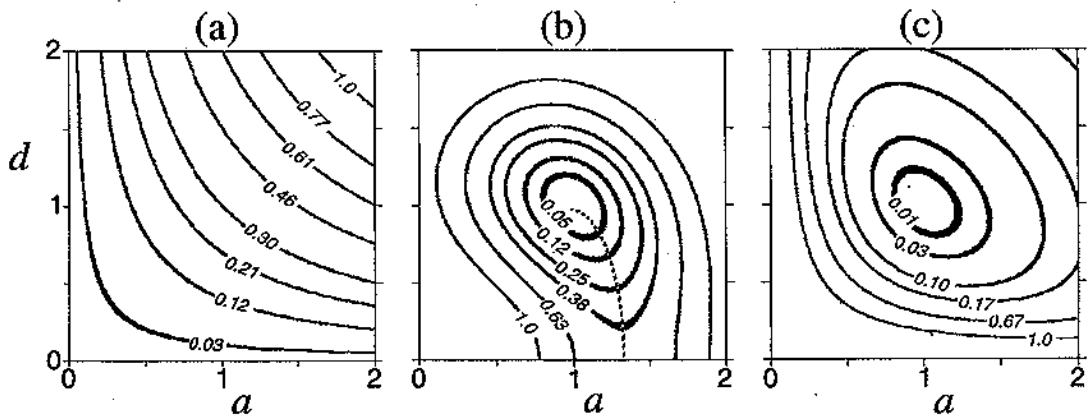

FIG. 4. Strain energy contours at zero temperature as a function of the biaxial deformation variables a and d. The energy scale is arbitrary. (a) Pressure times area. (b) Hookean spring model. (c) Polymer net model. The dashed curve in (b) approximates the transition trajectory to the a-axis boundary when compression is applied to the Hookean spring model; a saddle-point barrier energy lies midway between the two endpoints.

perature range $T>0$. Nets are placed in a periodic box of reference dimensions $L_Y \times L_X$: an $M \times M$ array of $N=M^2$ vertices has a rectangular reference size $L_Y = M(\sqrt{3}/2)S_{\rm ref} \times L_X = MS_{\rm ref}$. In biaxial deformation, $a = L_x/L_X$ and $d = L_y/L_Y$. Both the positions of the vertices themselves, as well as the box shape and dimension, change during the Monte Carlo simulation. Each attempt to move a particle to a different position, or change the value of L_x or L_y, or the angle between the sides, is accepted or rejected according to the usual stress ensemble Boltzmann weight. The same basic procedure has been used previously to determine average properties, e.g., $\langle A \rangle$, and fluctuation properties, e.g., $K_a/k_BT = \langle A \rangle / (\langle A^2 \rangle - \langle A \rangle^2)$, of networks under isotropic tension [9]. Further details on algorithms and methodology can be found in Appendix B of this paper and the appendices of Ref. [9].

III. HOOKEAN SPRING NETWORKS

In this section we focus on Hamiltonians of Eq. (5), where $S_0>0$ and $f(\bar{\rho})=0$. We report results for several values of the power-law exponent n, but give most attention to Hookean spring networks which are defined by $n=2$ (see Fig. 3). It is further assumed for now that $S_0 = S_{\rm ref}$.

A. $T=0$ deformation energy

For this Hookean spring network, the $T=0$ strain energy surface (with $b=c=0$) is shown in Fig. 4(b): note the distinctive asymmetry about the line $a=d$. In biaxial deformation, the implicit square root in the *exact* strain energy of Eq. (6) is expanded [29] about the reference state of $(a=\lambda_1) = (d=\lambda_2) = 1$ to yield

$$\tilde{W}/(k_{\rm sp}\sqrt{3}) = \tfrac{1}{8}(3E_{11}^2 + 2E_{11}E_{22} + 3E_{22}^2) - \tfrac{1}{32}(11E_{11}^3 + 9E_{22}^3 + 3E_{11}^2E_{22} + 9E_{22}^2E_{11}) + O(E^4). \tag{9}$$

Anisotropy is evident at third order (e.g., unequal coefficients for E_{11}^3 and E_{22}^3). It follows that there must be a cubic term in η_2. Indeed, in terms of the η's [Eq. (2)] or C_6-invariants [Eq. (3)] and for a *completely arbitrary* deformation

$$\begin{aligned}\tilde{W} &= \tfrac{1}{2}K_a^0\eta_1^2 + \tfrac{1}{2}\mu^0(2\eta_2^2 + 4\eta_3^2) - \tfrac{1}{8}(k_{\rm sp}\sqrt{3})[4\eta_1^3 + 2\sqrt{2}\,\eta_2^3 \\ &\quad + 12\eta_1\eta_2^2 + 24\eta_1\eta_3^2 - 12\sqrt{2}\,\eta_2\eta_3^2] + O(E^4) \\ &= \tfrac{1}{2}K_a^0 I_1^2 + \tfrac{1}{2}\mu^0(I_1^2 - 4I_2) - \tfrac{1}{8}(k_{\rm sp}\sqrt{3}) \\ &\quad \times [9I_1(I_1^2 - 4I_2) + 2I_3] + O(E^4),\end{aligned} \tag{10}$$

In Eq. (10), the surface bulk and shear moduli are identified at $P=0$ (superscripts denote $T=0$) as $K_a^0 = \frac{1}{2}(C_{1111} + C_{1122}) = \frac{1}{2}[(\lambda^0 + 2\mu^0) + \lambda^0] = \frac{1}{2}k_{\rm sp}\sqrt{3}$, and $\mu^0 = \frac{1}{2}(C_{1111} - C_{1122}) = \frac{1}{4}k_{\rm sp}\sqrt{3}$. These give $K_a^0/\mu^0 = 2$, a well-known result for two-dimensional (2D) triangular nets of harmonic springs. Hence the symmetry at the order of the quadratic strain in Eq. (9) is captured in Eq. (10) with an isotropic surface response; i.e., the quadratic terms are accounted for with I_1 and I_2 [30]. Third-order terms in strain arise from I_1 as well as I_2, but these contributions are always symmetric (i.e., permutable in E_{IJ}); the invariant I_3, characteristic of the sixfold symmetry of the network breaks the symmetric response at this order, and is directly responsible for the presence of the term η_2^3. Of importance to analyses in Sec. IV and in contrast to developments above, the irreducible quadratic form of the strain energy for a planar structure of C_2 symmetry generally has four rather than just two distinct coefficients in

$$\tilde{W} = \frac{1}{2!}C_{1111}E_{11}^2 + \frac{1}{2!}C_{2222}E_{22}^2 + C_{1122}E_{11}E_{22} + 2C_{1212}E_{12}^2 + O(E^3). \tag{11}$$

B. Phase transition in compression

It has been shown [9] that, at low temperature, a spring network under tension is well described by a mean-field model in which all springs have the same length $S = |\mathbf{r}_{01}| = |\mathbf{r}_{02}| = |\mathbf{r}_{03}|$, i.e., *equilateral* triangles. The zero-temperature surface bulk and shear moduli in this mean-field model are given fully as a function of pressure by

$$K_a^0/k_{\rm sp} = \frac{\sqrt{3}}{2}\{1 + P/\sqrt{3}k_{\rm sp}\}, \tag{12a}$$

$$\mu^0/k_{\rm sp} = \frac{\sqrt{3}}{4}\{1 - \sqrt{3}P/k_{\rm sp}\}, \tag{12b}$$

while the zero-temperature area per triangle is

$$\langle A \rangle^0 = (\sqrt{3}/4)S_0^2/\{1 + P/\sqrt{3}k_{\rm sp}\}^2. \tag{12c}$$

From Eq. (12a), K_a^0 vanishes at the isotropic tension $-k_{\rm sp}\sqrt{3}$, and the network area expands without bound asymptotic to this tension.

Keeping in mind the key assumption that Eqs. (12) apply to homogeneous networks of *equilateral* triangles, the infinitesimal shear modulus μ^0 is seen to vanish under compression at $P = k_{\rm sp}/\sqrt{3}$ and $S = \frac{3}{4}S_0$. However, if one now considers microstates other than equilateral triangles, then, at a much smaller compression of $P^* = (\sqrt{3}/8)k_{\rm sp}$ the free energy will be minimized with a network area of zero, such that the value of the pressure-area contribution vanishes. *Each plaquette becomes a line.* Just below P^*, the ground-state plaquette is an equilateral triangle of side $\frac{3}{4}S_0$; just above P^*, this changes to a "crushed" isosceles triangle with two sides of length $\frac{2}{3}S_0$ and one side of length $\frac{4}{3}S_0$, as shown in Fig. 5(a). In the combined free-energy surfaces of Figs. 4(a) and 4(b), which together represent Eq. (7), the ground state is shifted from the symmetric configuration $a=d=1$ at small P to the global energy minimum at $d=0$, $a=\frac{4}{3}$ when the pressure exceeds P^*. Importantly, at the transition and when $b=0$, (i) η_3 does not change, (ii) η_1 is a^2 in the equilateral state and $\frac{1}{2}a^2$ in the crushed state, and (iii) η_2 is 0 in the equilateral state and $(\sqrt{2}/4)a^2$ in the crushed state. Thus η_2 is the candidate order parameter most appropriate to this transition. Note that the crushed state is a "boundary state" with nonzero gradients in strain energy.

The $T=0$ energy surfaces defined by the progressive expansion in Eq. (10) show that the quadratic terms in the strain, i.e., the isotropic terms, make the crushed state a glo-

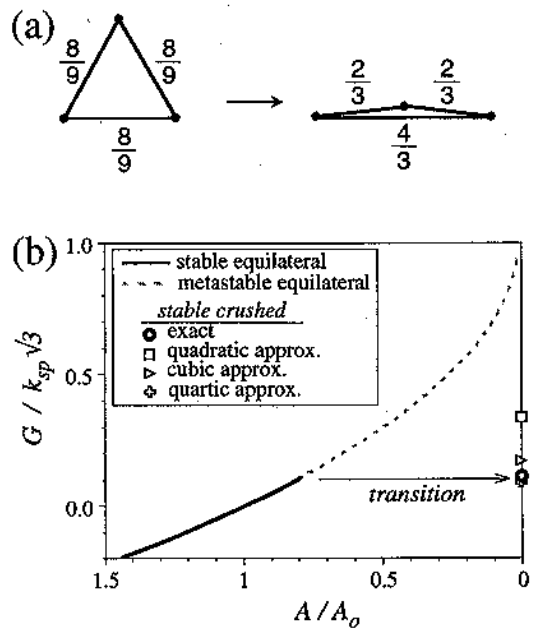

FIG. 5. C_6–C_2 transition of Hookean spring model at zero temperature. (a) The ground-state plaquette is an equilateral triangle above P^* and a "crushed" isosceles triangle below P^*. Numbers refer to the length of the indicated side scaled by S_0. (b) Free energies of the plaquette under compression.

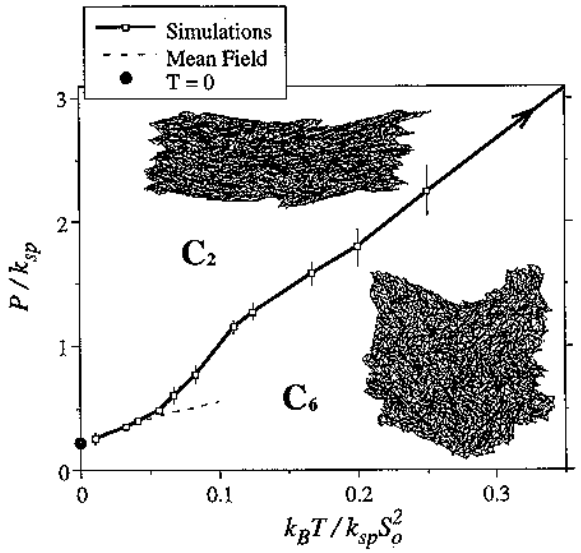

FIG. 6. Phase boundary in the pressure-temperature plane for Hookean spring networks under compression. The arrow points toward a data point at $k_BT/k_{sp}S_0^2=1$. The dashed line refers to the $T=0$ model, where an ideal gas entropy has been added. The solid lines through the simulation data are drawn to guide the eye. The two inset sample configurations of a large Hookean spring net at a moderately high temperature ($N=48^2$; $k_BT/k_{sp}S_0^2=\frac{1}{5}$) are shown at pressures just below and just above the transition ($P/k_{sp}=1.8$ and 2, respectively); the periodic box is hidden from view.

bal minimum [see Fig. 5(b)] under suitable compression. The crushed state is threefold degenerate $\{(a,b,d)$: $(\frac{4}{3},0,0)$, $[\frac{2}{3},0,\pm(2/\sqrt{3})]\}$, rather than sixfold, as determined through the asymmetry of the C_6 invariant I_3. Furthermore, given the η_2^3 term in the energy that results from I_3, this symmetry-breaking crushing transition must be a first-order transition in the context of a Landau theory [17]. This may be expected to hold true regardless of temperature since, near the transition, the most important η_2 contributions to the free energy sum to

$$A(P,T)\eta_2^2+B(P,T)\eta_2^3+C(P,T)\eta_2^4+\cdots , \qquad (13)$$

and since $A(P,T)$ *but not* $B(P,T)$ will vanish at the transition. In the (P,T) plane, the phase boundary should thus appear like the liquid-solid or isotropic-nematic lines in lacking a critical point at any finite (P,T).

In many martensitic transitions, density changes occur without driving the transition, but they nonetheless clearly signal the transition [19]. For the current Hookean spring model, area versus pressure isotherms crossing a coexistence region were described at the outset with Fig. 1(b). At low temperature, the transition pressure for the discontinuous martensitic-like transformation is modeled well (Fig. 6) simply by destabilizing the "crushed" phase with the free-energy (entropy) change for an ideal gas of network nodes. Thus, in much the same way as was done in early models of polymer networks [20,21], the vertices are considered a gas of fluctuating nodes, so that

$$\tilde{G}_{T>0}\approx\tilde{G}_{T=0}+\rho_0 k_B T \ln\bar{\rho}. \qquad (14)$$

The quantity ρ_0 is the number of nodes per area at zero pressure and temperature, i.e., $N/A_{T=0}$. This ideal gas entropy change term, it may be remarked, also can be derived as the $O(T)$ term [22] in the equilateral triangle version of Z_P reduced from Eq. (8). Motivation for this approximation is provided in part by the apparent randomness in the sample configurations of the network near the transition as shown in Fig. 6.

Although the mean-field expression for equilateral triangles provides a reasonably good description of the network area under moderate tension for low temperatures, network compression is more difficult to predict quantitatively even with the more general partition function of Eq. (8). As an example of the difficulty, the inset to Fig. 1(b) for $\langle A\rangle_0$ vs temperature demonstrates a feature atypical of solids: the stress-free area decreases as the temperature is initially increased from zero. Near $k_BT/k_{sp}S_0^2\approx 0.2$, a minimum is reached, and, above this temperature, network area grows asymptotic to the linear scaling expected of ideal gas behavior. Such a negative coefficient of thermal expansion at small temperatures is well known for pure ice near zero K [23], and is also expected of a 1D polymer under a near-zero force [24]. The single-plaquette, mean-field integral of Eq. (8) shows the same qualitative behavior. The initial downward trend in area seems due to the very "open" low-temperature structure, like the H-bonded networks in ice, which allow for a predominance of internal thermal motions. Entropic filling of interstitial voids reverses the trend in these spring networks, and gives way eventually to an ideal gas of network nodes in the high temperature limit.

Networks at infinite temperature ($k_{sp}=0$) can be investigated only for $P>0$. Simulated networks in this limit show that $P\langle A\rangle/N=k_BT[1+O(1/N)]$, $K_a=P$, and the Young's moduli vanish ($N=8^2$, 12^2, 20^2, 24^2, or 30^2). This implies

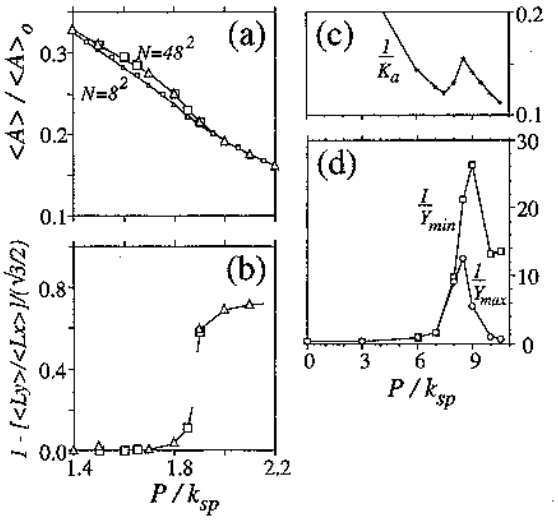

FIG. 7. Hookean spring networks under compression at high temperatures. (a) and (b) area and Bain-type order parameter, respectively, at $k_BT/k_{sp}S_0^2=5$ for $N=48^2$ (squares) or 8^2 (triangles). (c) and (d) Elastic moduli as a function of pressure at $k_BT/k_{sp}S_0^2=1$ for $N=64^2$. The configuration space is threefold degenerate, and the simulation time needed to move among the degenerate regions is large. Hence our ensemble is constructed from post-relaxation steady states which fluctuate about one of the three degenerate regions. Y_{max} and Y_{min} in (d) are essentially Y_Y and Y_X except for the last data point, which is reversed. The solid lines through the simulation data are drawn to guide the eye.

that the three-particle constraint $\mathbf{z}\cdot(\mathbf{r}_{ij}\times\mathbf{r}_{ik})>0$ does not contribute to the average internal virial; ideal behavior is expected here because there is no excluded volume (nor attraction) with this signed-area steric interaction between infinitely thin tethers. In spite of the ideal gas behavior at high temperature, the constraint on the signed area is crucial to stability against network collapses at $P=0$: a "phantom" network (lacking the signed area constraint) collapses at the remarkably low temperature of $k_BT/k_{sp}S_0^2\sim 1/20$ [25].

We have shown above that the phase transition to the crushed state is present at $T=0$, but is absent at infinite temperature. At intermediate temperatures, between zero and $k_BT/k_{sp}S_0^2\approx 0.1$, distinct hysteresis loops in the network area define a coexistence region [Fig. 1(b)], and the hysteresis increases with system size, consistent with the first-order nature of the phase change. For fixed T, the transitions, even from metastable states, also sharpen with increased network size. Away from the transition region, finite-size effects are negligible. All of these effects can be seen in Fig. 1(b). Parenthetically, if one calculates a Hookean spring constant from the in-plane "shear modulus" often attributed to the red cell cytoskeleton [4], ignoring all questions of appropriateness, the relevant isotherms are among those between $k_BT/k_{sp}S_0^2=\frac{1}{18}$ and $\frac{1}{100}$ [26]. Phase transitions, hysteresis, and all the associated difficulties are quite prominent in this temperature range. At still higher finite temperatures, the change in network area across the transition is found to be a very small fraction of the unstressed area and is difficult to detect even for large systems [Figs. 7(a) and 7(c)]; however, according to the Clausius-Clapeyron equation, both ΔA and the entropy change across the transition can be small but cannot vanish (in the thermodynamic limit) when the phase boundary's slope dP^*/dT is finite, as seen in Fig. 6. Indeed, the transition is better identified by a deviation from zero of the Bain-type order parameter $1-\langle a\rangle/\langle d\rangle$ [Fig. 7(b)] [6,7], which is related to η_2. Furthermore, while the transition from C_6 is always marked by the vanishing of μ^0 as the quadratic coefficient $A(P,T)$ for η_2^2, the symmetry breaking to C_2 is also characterized by divergences in the inverse Young's moduli, $C^{-1}_{1111}=C^{-1}_{2222}$, coincident with a growing nonzero difference in their values [Fig. 7(d)]. This is consistent with the disparity in the quadratic order terms of a C_2 energy [Eq. (11)].

We conclude this section by returning to the general form of H in Eq. (5) which admits n-monic springs (Fig. 3). It is found at $T=0$ that the crushing transition described above for Hookean springs ($n=2$) also occurs for larger n, up to at least $n=40$. The smallest, stable equilateral triangle has an elemental length S/S_0 of $\frac{8}{9}$ ($n=2$) which decreases quickly and levels off at $\sim\frac{3}{4}$ ($n=40$). Further investigations of the properties of n-monic springs at nonzero temperatures will not be reported here.

IV. SQUARE-WELL NETWORKS

In the limit of the exponent n approaching infinity, the n-monic Hamiltonian [with $S_0>0$ and $f(\bar{p})=0$ in Eqs. (5) and (6)] looks like a square well ($S_{max}=2S_0$ as $n\to\infty$), wherein the stretching energy of a spring rises rapidly from zero as the spring length exceeds some constant S_{max} [9]. With the pure square-well model, there is no intrinsic energy scale, and the properties of the network depend on the applied pressure and the presence (or absence) of self-avoidance. The limits to the Z_P integrations of Eq. (8) are precisely defined for square-well potentials, and the properties of the single plaquette can be determined exactly at $P=0$:

$$Z_P=\tfrac{1}{48}(12\pi-9\sqrt{3}) \tag{15a}$$

$$\langle S\rangle_0/S_{max}=2\left(\frac{\pi}{18}+\frac{16}{45}-\frac{9\sqrt{3}}{40}\right)\Big/ Z_P=0.609\ldots, \tag{15b}$$

$$\langle A\rangle_0/A_{max}=\tfrac{15}{288}/Z_P=0.261\ldots, \tag{15c}$$

$$K_{a,0}S_{max}^2/k_BT=\tfrac{1}{128}\left(\pi-\frac{9\sqrt{3}}{8}\right)\Big/ Z_P=7.589\ldots . \tag{15d}$$

These average and fluctuation quantities are in remarkable agreement with simulations of the full network which yield $\langle S\rangle_0/S_{max}=0.604$, $\langle A\rangle_0/A_{max}=0.247$, and $K_{a,0}=8.5\pm 0.5$. Furthermore, the probability distributions for either the sides or areas of triangles in a network are found to be very similar in shape to those of a single plaquette. These results suggest that neighboring triangles in a square-well net, after an ensemble average, are nearly invisible to each other.

A. Compression

Square-well nets share some, but certainly not all, features of harmonic nets [9]. A harmonic spring network with the

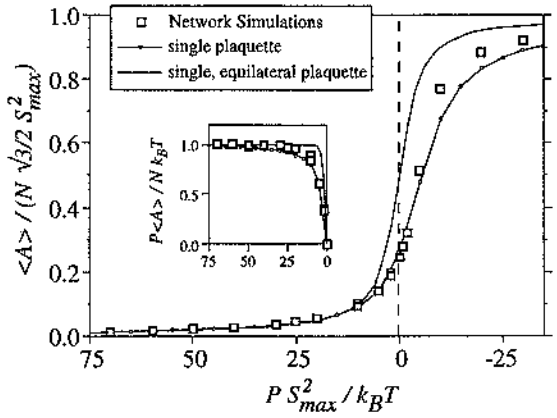

FIG. 8. Area as a function of pressure for square-well network and single plaquette mean-field models. The inset compares results for compression to ideal gas behavior where $P\langle A\rangle = Nk_BT$. Several network sizes, from $N=12^2$ to 64^2, were used over the entire range of compression, and indicated no particular size dependence.

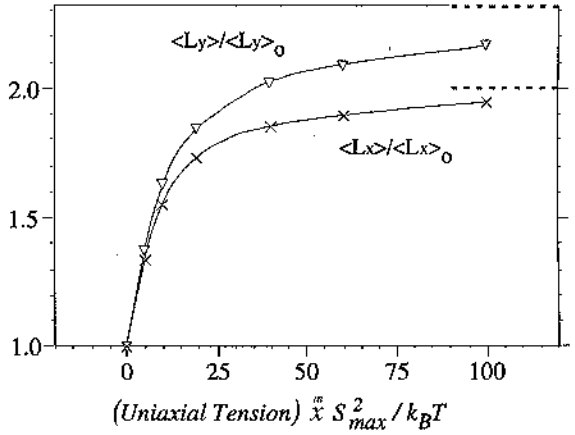

FIG. 9. Stretch in the Y or X direction, when uniaxial tension is applied to square-well networks in either one of these directions. The slope near zero uniaxial tension gives a single Young's modulus, in close accord with that determined by fluctuations at $P=0$. The solid lines through the simulation data are drawn to guide the eye.

same $K_{a,0}$ and $\langle S\rangle_0/S_{\max}$ as Eqs. (15b) and (15d) would be expected to have a temperature in the range $k_BT/k_{sp}S_0^2 \approx 2$ to 4. Such a spring network would show a transition at $PS_{\max}^2/k_BT$ of order 20. However, simulations of square-well networks under an applied pressure exhibit no transition for compressions up to at least $PS_{\max}^2/k_BT=80$, where $\langle A\rangle/\langle A\rangle_0 \sim 0.060$ (Fig. 8). For comparison of these numbers to a Hookean spring model, the C_6-C_2 transition at the high temperature of $k_BT/k_{sp}S_0^2=1$ occurred at $\langle A\rangle/\langle A\rangle_0 \approx 0.11$.

Of greater importance, square-well networks under significant pressures ($PS_{\max}^2/k_BT \gtrsim 20$) exhibit ideal gas behavior: $P\langle A\rangle \approx Nk_BT$ (Fig. 8, inset) and $K_a \approx P$. At these pressures, the probability of a tether being within 10% of $S_{\max}$ is exceedingly small. Thus, as with the $k_{sp}=0$ Hookean spring net, the only intrinsic length scale in the net ($S_{\max}$ here) is unimportant under high compression. Indeed, for a similar reason, the one-dimensional form of the mean field Z_P [Eq. (8)], i.e., considering only equilateral triangles, also yields ideal gas behavior in the high compression limit:

$$\langle A\rangle = (k_BT/P)[1+\chi/(1-e^{\chi})] \rightarrow k_BT/P \quad \text{as} \quad P\rightarrow+\infty \tag{16a}$$

$$K_a = P/\{1-[\chi/(1-e^{\chi})][1-e^{\chi}+\chi e^{\chi}]/[1-e^{\chi}+e^{\chi}]\} \rightarrow P \quad \text{as} \quad P\rightarrow+\infty. \tag{16b}$$

In these equations $\chi = PA_{\max}/k_BT$, where $A_{\max}=(\sqrt{3}/2)S_{\max}^2$. Graphical comparisons of simulated nets and the single-plaquette models are made in Fig. 8.

B. Anisotropy

Despite the evident lack of symmetry breaking or collapse under compression, the square-well network, like the n-monic nets, still exhibits anisotropies. Under uniaxial tension in the X or Y directions stretch as a function of uniaxial tension for square-well nets displays distinct asymptotes (Fig. 9). The ratios of the maximum to initial lengths in the X and Y directions are $S_{\max}/S_0$, and $2S_{\max}/\sqrt{3}S_0$, respectively; hence the maximum strain in the X direction is smaller than that in the Y direction simply by the ratio $(\sqrt{3}/2)$. This anisotropy is a very simple but general consequence of tether limits in the triangular geometry.

V. THREE-BODY ENERGETICS: "FLORY NETWORKS"

Sections III and IV dealt with networks having strictly two-body interactions constrained only by the requirement that the three-body signed area of each plaquette not change. We now generalize this to include a less trivial form for the three-body interaction term in the Hamiltonian of Eq. (5). Such an interaction may help provide a very elementary representation of quasi-two-dimensional, cytoskeletonlike triangular nets assembled from linear polymers rather than simple springs [26]. With the assignment $S_0=0$ and $n=2$, the initial term of the Hamiltonian [Eq. (5)] becomes Gaussian, and, in neglecting the explicit summation over the network vertices, therefore polymer-like [12,21,27]. The effective spring constant k_{sp} would be dependent on monomer number, temperature, etc. Furthermore, monomers of the polymer chains fluctuate locally, it is envisioned, to fill the interstitial A_{ijk} of the net. As in the typical Flory argument [27], correlations are neglected in assuming that such filling is spatially uniform within each triangle. This assumption leads to a nonzero three-body term $f(\bar{\rho})\neq 0$ and the name "Flory-polymer net" or simply "Flory net."

In choosing $S_0=0$, $n=2$, and $f(\bar{\rho})\neq 0$, the exact strain energy of Eq. (6) appears expressible strictly in terms of *isotropic* surface quantities $\mathrm{tr}\Lambda^2$ and $\bar{\rho}$,

$$\tilde{W} = (k_{sp}\sqrt{3})\tfrac{1}{2}\mathrm{tr}\Lambda^2 + f(\bar{\rho}). \tag{17}$$

Derivatives of the first term yield $\mu=\mu^0=k_{sp}\sqrt{3}$. It proves convenient now to define the invariants J_1, J_2, and J_3 formally by simply replacing $\mathbf{E}$ with Λ^2 in Eqs. (3), e.g., $J_1 = \mathrm{tr}\Lambda^2 = (a^2+c^2+b^2+d^2)$. Each invariant of the set J_i vanishes when the deformation map is the null tensor rather than the identity so that, in the case of no applied stress, $\bar{\rho}=1$ and $J_1=2$. Figure 4(c) shows the strain energy surface for this

model in biaxial deformation with a particular choice for $f(\bar{\rho})$ elaborated below. The symmetry about $a=d$ is a generic feature of Eq. (17). For comparison to Hookean springs, Fig. 3 (right-hand side) maps the same sum of energies into an effective elemental potential.

Toward assigning $f(\bar{\rho})$, we assume that the osmotic pressure Π in the polymer net depends on local monomer density as $\Pi=\Pi(\bar{\rho})$, and that the constraints of network connectivity condense the network sufficiently into the nondilute polymer melt regime to give

$$f(\bar{\rho})=B_1\bar{\rho}+B_2\bar{\rho}^2+\text{const.} \tag{18}$$

If the dominant osmotic term in this is the B_1 term, then a balance of chain elasticity against excluded volume (*à la* Flory polymer chains) allows one to determine $B_1=\frac{3}{2}k_{sp}S_{ref}^2$ and $K_a^0=2k_{sp}\sqrt{3}$ at $P(\bar{\rho}=1)=P_{ext}=0$. Hence $K_a^0/\mu^0=2$ so that, at this order, the network looks very much like a network of Hookean springs. However, this Flory net is rigorously isotropic in its mechanical responses. These features appear consistent with simulations of cytoskeletal polymer nets tacked to a bilayer wall [27] within the approximate range $0.5\lesssim\bar{\rho}\lesssim 2.5$, in spite of the very gross simplifications of our Flory net calculation. Additionally, recent experiments which reveal red cell cytoskeletal network deformations [3] have been shown to be fit reasonably well, at least by axisymmetric continuum analyses, with an isotropic strain energy expression which can be built in part from Eqs. (17) and (18). In [3], the strain energy is denoted as E_{net} instead of $\tilde{W}$, and a function $g(\bar{\rho})\sim 1/\bar{\rho}^2$ is included:

$$E_{net}=\tfrac{1}{2}\mu(\lambda_1^2+\lambda_2^2)+B_1\bar{\rho}+g(\bar{\rho}). \tag{19}$$

The first term is just the 2D form [4] of the classic 3D rubber elasticity strain energy, which merely includes λ_3^2 in the sum over squared stretches, as established by Flory and others (for example, [16,20,21]). The shear modulus μ in these latter microscopic theories is given by the product of k_BT and the number of chains per area (2D) or volume (3D); in such a case, the spring constant appropriate for the mesoscale triangular Flory nets is $k_{sp}=\mu/\sqrt{3}$.

Importantly, because $S_0=0$ in the Flory net elements, there is no symmetry in the elemental energetics, and therefore no discontinuous "crushing" transition in these types of nets (Fig. 10). Any decrease in network area is continuously opposed by a soft-core repulsion reflecting the fluctuating monomer interactions. However, in positive tension ($P<0$) the area of this harmonic Flory net along with the length of each linear element increases without bound asymptotic to a finite tension $P_{T=0}=k_{sp}\sqrt{3}(\bar{\rho}^2-1)\to -k_{sp}\sqrt{3}$, just as with nets of Hookean springs [9] [note that Eq. (12c) is equivalent to $P_{T=0}=k_{sp}\sqrt{3}(\bar{\rho}^{1/2}-1)$] and harmonic potential 2D ring polymers [28]. Considering, then, that basic linear elements of physical networks like the cytoskeleton are often polymers which have a maximum length S_{max}, there should be a limit to the stretching of nets, similar to our square-well networks. This effect is certainly observable in a recent cytoskeleton computer simulations [26]. We therefore assume here that the free energy stored in the length of each "polymerlike" element can be approximated by an expansion beyond the Gaussian term to give the effective Hamiltonian

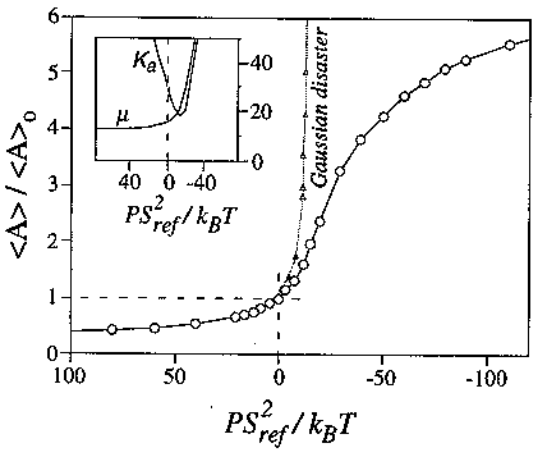

FIG. 10. Flory nets under isotropic pressure at finite temperature: $k_BT/k_{sp}S_{ref}^2=\frac{1}{8}$. Inset and open circles show simulation results for an anharmonic model which approximates more microscopic cytoskeleton simulations [26]. The solid line through the simulation data is drawn to guide the eye.

$$H=\frac{1}{2!}\sum_{ij}^{net}(\tfrac{1}{2}k_{sp}S_{max}^2)[(\mathbf{r}_{ij}\cdot\mathbf{r}_{ij}/S_{max}^2)+\phi_2(\mathbf{r}_{ij}\cdot\mathbf{r}_{ij}/S_{max}^2)^2 +\phi_3(\mathbf{r}_{ij}\cdot\mathbf{r}_{ij}/S_{max}^2)^3+\cdots] +\frac{1}{3!}\sum_{ijk}^{net}\frac{3}{2}k_{sp}S_{ref}^2\left[\sum_n n\phi_n(S_{ref}^2/S_{max}^2)^n\right](A_{ref}/A_{ijk}). \tag{20}$$

For freely jointed polymer chains in three dimensions, the familiar inverse Langevin function approach [16] yields $\phi_2=\frac{3}{10}$, $\phi_3=\frac{33}{175}$, etc. To third order in the invariants of Λ^2, the strain energy is

$$\tilde{W}/(k_{sp}\sqrt{3})=\tfrac{1}{2}J_1+\tfrac{1}{2}\phi_2(S_{ref}^2/S_{max}^2)(\tfrac{3}{4}J_1^2+J_2) +\tfrac{1}{32}\phi_3(S_{ref}^2/S_{max}^2)^2(9J_1^3-54J_1J_2+2J_3)+\cdots +\left[\sum_n n\phi_n(S_{ref}^2/S_{max}^2)^{n-1}\right]\bar{\rho}. \tag{21}$$

The anharmonic terms in $\mathbf{r}_{ij}\cdot\mathbf{r}_{ij}$ stabilize a network under positive tension (e.g., Fig. 10). The ϕ_3 term is the first to introduce the third-order invariant J_3, so that, like the square-well networks in uniaxial tension, these anharmonic Flory nets are anisotropic at and above this order. The virial coefficient of the density function may now also depend on the higher-order terms and, though this dependence falls off quickly with large S_{max}/S_{ref}, issues of convergence need be considered. In the end, the anisotropy introduced by "polymer-length" limits and the absence of a $g(\bar{\rho})\sim 1/\bar{\rho}^2$ term in Eq. (21) distinguish it from the simpler, isotropic expression [Eq. (19)] already used to fit the red cell experiments [3]. This anisotropy, it should be emphasized, makes it impossible to rigorously apply the aforementioned axisymmetric analyses to nonhomogeneous cell deformation.

VI. CONCLUSIONS

The large deformation, in-plane responses of several perfect triangular network models have been determined. For nets assembled simply from central force springs (force-free length>0), a discontinuous transition under compression is demonstrated, in which the C_6 symmetry of the network is reduced to C_2. No transition under compression is observed, however, when this force-free length scale, which sets a symmetry in the interaction potential, is eliminated and when one of the following apply: (i) $T\rightarrow+\infty$; (ii) the continuous potential is replaced with a square-well; and (iii) the elemental elasticity is balanced against local, mean-field sterics, to mimic a polymerlike net. For conditions (i) and (ii), the limiting behavior in compression is that of an ideal gas which can reflect only the signed area constraint. For the models of (iii), the compression limit leads to a non-ideal gas determined by the assumed form of supplemental sterics. In spite of such rotationally invariant limit states, nonsymmetric responses of triangular nets are more typical, and the phase transition is but one manifestation of this. Uniaxial tension of triangular nets with any sort of maximum tether length also clearly leads to an anisotropic response with the associated odd-order elastic constants. To uncover these effects experimentally, the phase transitions and anisotropies in some of the sixfold structures listed at the outset of this paper comprise the logical next step.

Note Added. After submitting this manuscript, we received a preprint from Wintz, Everaers, and Seifert, who also observed a collapse transition in 2D triangular networks. They used a fixed area ensemble, and their equation of state agrees approximately with ours over the range of network areas reported in their paper: $A_{\rm net}/A_{T=0}>0.5$, where $A_{\rm net}$ is the network area. The phase transitions seen in our own simulations of Hookean spring nets in a fixed pressure ensemble extend below this range, as shown in our Fig. 1(b).

ACKNOWLEDGMENTS

This work was supported in part by the Natural Sciences and Engineering Research Council of Canada and by the U.S. National Science Foundation. Discussions with P. Lammert are very gratefully acknowledged.

APPENDIX A

Considering a biaxial deformation, the exact strain energy density of the large class of nets represented by Eq. (6) reduces to

$$\tilde{W}=\left[\frac{2}{n}k_{\rm sp}/\sqrt{3}\right]\{2[\tfrac{1}{2}(\lambda_1^2+3\lambda_2^2)^{1/2}-(S_0/S_{\rm ref})]^n + [\lambda_1-(S_0/S_{\rm ref})]^n\}+f(\bar{\rho})/(S_{\rm ref}^2\sqrt{3}/2). \quad \text{(A1)}$$

Tensions in the network may then be calculated from $T_1=(1/\lambda_2)\partial\tilde{W}/\partial\lambda_1$ and $T_2=(1/\lambda_1)\partial\tilde{W}/\partial\lambda_2$. As an aside, simple shearing in a continuum sense may appear removed upon setting $b=0$; however, material shearing still can be isolated in a state where $\lambda\equiv\lambda_1=1/\lambda_2$, a state referred to as pure shear. For this state, a shear strain may be identified, though not uniquely, as $E_s\equiv\frac{1}{2}(\lambda^2-1/\lambda^2)$ [4]. By calculating a shearing tension $T_s\equiv\frac{1}{2}|T_1-T_2|$, a shear modulus in large deformation elasticity can be obtained as $\mu\equiv T_s/E_s$. With this choice of E_s, the proper infinitesimal identification of the shear modulus generally can be regained in the small strain limit. For the strict Hookean spring network, it is apparent that λ_1 and λ_2 do not permute in the strain energy expression Eq. (22); such a network is therefore anisotropic.

APPENDIX B

An ensemble of configurations is generated by the Monte Carlo procedure for each chosen combination of parameters such as N, $k_{\rm sp}$, and P. Typically, the ensemble represents at least 2×10^6 moves per particle after the system is allowed to relax from its initial configuration. Of course, successive configurations in the ensemble are correlated, and so the number of statistically independent configurations is considerably less than two million, depending on system parameters. The ensemble is used to calculate averages such as the area $\langle A\rangle$ directly, and to calculate the elastic moduli indirectly through lowest-order fluctuations. The moduli also were obtained from full strain-strain correlations as a check on the accuracy of the technique. With Hookean spring networks, the average energy per nodal particle in nets under no stress was essentially two times $\frac{1}{2}k_BT$ and, by calculating the in-plane virial stresses, we observed that $T_{\rm ext}-\langle T_{\rm int}\rangle\approx0$. For simulations of uniaxial tension, stress was applied to just two parallel faces of the periodic box and collective moves made accordingly. We estimate that the uncertainties in ensemble averages such as $\langle A\rangle$ are less than 1%, and that the uncertainties in the moduli are less than 5%. Further details on algorithms and methodology can be found in the appendices of Ref. [9].

[1] L. D. Landau and E. M. Lifshitz, *Theory of Elasticity* (Pergamon, London, 1959), Chap. I.

[2] T. J. Byers and D. Branton, Proc. Natl. Acad. Sci. U.S.A. **82**, 6153 (1985); note that the red cell cytoskeleton has on the order 3×10^4 network nodes. The largest planar system we have studied is a fraction of this.

[3] D. E. Discher, N. Mohandas, and E. A. Evans, Science **266**, 1032 (1994).

[4] E. A. Evans and R. Skalak, *Mechanics and Thermodynamics of Biomembranes* (CRC, Boca Raton, FL, 1980).

[5] D. H. Pearson and R. J. Tonucci, Science **270**, 68 (1995).

[6] J. A. Krumhansl, J. Phys. (Paris) Colloq. **5**, C2-3 (1995).

[7] P. W. Anderson and E. I. Blount, Phys. Rev. Lett. **14**, 217 (1965).

[8] Z. Fan, L. Xiao, and Z. Jinxiu, Phys. Rev. Lett. **77**, 1394 (1996).

[9] D. H. Boal, U. Seifert, and J. C. Shillcock, Phys. Rev. E **48**, 4274 (1993).